International Journal of Heat and Mass Transfer 127 (2018) 806–817

Contents lists available at ScienceDirect

International Journal of Heat and Mass Transfer

journal homepage: www.elsevier.com/locate/ijhmt

Influence of wettability due to laser-texturing on critical heat flux in vertical flow boiling

Joseph L. Bottini, Vineet Kumar, Sabrina Hammouti, David Ruzic, Caleb S. Brooks *

Department of Nuclear, Plasma, and Radiological Engineering, University of Illinois, Urbana, IL 61801, USA

ARTICLE INFO

Article history:
Received 30 March 2018
Received in revised form 21 June 2018
Accepted 21 June 2018

Keywords:
Critical heat flux
Wettability
Flow boiling
Departure from nucleate boiling

ABSTRACT

The critical heat flux (CHF) marks the upper limit of safe operation of heat transfer systems that utilize two-phase boiling heat transfer. In a heat-flux-controlled system, exceeding the CHF results in rapid temperature excursions which can be catastrophic for system components. Recent studies have focused on the influence of surface wettability on the departure from nucleate boiling (DNB) through surface modifications and coatings, though many of these studies are limited to pool boiling systems. In this study, the surface wettability influence is studied on the boiling curves and specifically the point of DNB. A femtosecond laser is used to texture the surface to change the wettability from hydrophilic to hydrophobic. A parametric study is performed with mass flux, pressure, and inlet subcooling in a vertical rectangular channel that is heated from one side. CHF excursions are triggered under various system conditions and are compared with existing models. For the experimental conditions considered, the hydrophobic surface showed delayed onset of nucleate boiling compared to the hydrophilic surface, shifting the boiling curves to higher wall superheat. The hydrophobic surface also showed significantly lower CHF for the same system conditions and less sensitivity to changes in subcooling.

1. Introduction

Boiling heat transfer is an effective cooling mechanism whereby large amounts of heat are removed from critical system components through the heating and vaporization of coolant, either driven by a pump or through buoyant forces. Boiling heat transfer offers high heat transfer coefficients due to both the sensible heating and the latent heating of the coolant, enabling high steady-state cooling rates with minimal surface superheats. The greatest concern of boiling heat transfer is the transition to poor heat transfer regimes, particularly the departure from nucleate boiling (DNB) to film boiling in low-quality flows and the dryout of the annular film in high-quality flows. These transitions are characterized by sudden temperature excursions which risk damage to components. For this reason, the critical heat flux (CHF) is a major safety concern in boiling heat transfer as well as a limitation for effective heat removal in many engineering applications. In addition, the sensitivity of wettability on the critical heat flux is an ongoing research effort for accident-tolerant fuels in nuclear power plants [1]. Due to the complexity of the phenomenon, the accurate prediction of CHF remains a concern [2–10].

Many studies have been conducted to experimentally measure and improve prediction of the critical heat flux in conditions relevant to commercial power generation, particularly in the nuclear industry where temperature excursions can lead to catastrophic system failures [11–14]. Experimental and modeling efforts [15–19] have led to understanding of triggering mechanisms for CHF, including bubble overcrowding, wetting fronts, Taylor instabilities, liquid sublayer dryout, and others. Particular attention has been given to addressing difficulties under low-pressure, low-flow conditions [2–9]. Mishima and Nishihara [2] analyzed the effect different geometries had on the CHF phenomenon, studying annuli, pipes, and square channels. For low-flow conditions, the CHF was found to approach the flooding limit due to the countercurrent-flow limitation proposed by Wallis [20] where the flow geometry was captured by a single constant. Chun et al. [3] and Schoesse et al. [4] also observed that the lower limit of CHF was captured by the flooding condition and that subcooling and pressure were less influential on the CHF in this low-flow regime. El-Genk et al. [5], Park et al. [6], and Kim et al. [7] all observed that, beyond the flooding limit (i.e., flow rates greater than 100–150 kg/m^2-s), the CHF increased with increasing pressure, mass flux, and subcooling. This effect was also observed by Chun et al. [3] which considers a wide range of pressures for CHF under low flow, observing that the peak in CHF occurred between

* Corresponding author at: Department of Nuclear, Plasma, and Radiological Engineering, University of Illinois, 104 South Wright Street, Urbana, IL 61801 USA.
E-mail address: csbrooks@illinois.edu (C.S. Brooks).

https://doi.org/10.1016/j.ijheatmasstransfer.2018.06.113
0017-9310/

Nomenclature

G	mass flux (kg/m^2-s)
P	pressure (kPa)
q''	heat flux (kW/m^2)
Re	Reynolds number (–)
ΔT	superheat or subcooling (°C)
t	time (s)

Greek

ε	error (–)

Subscripts

exp	experimental
mod	model
phil	hydrophilic
phob	hydrophobic
sub	subcooling
w	wall

2 and 3 MPa. Park et al. [6] and Kim et al. [7] both observed that the CHF also increased with increasing channel diameter and with decreasing heated length at constant mass flux. Lu et al. [8] and Mayer et al. [9] observed that the critical equilibrium quality decreased with increasing mass flux and decreasing pressure. Many studies that compare CHF data with existing models conclude that more research on CHF under low-pressure, low-flow conditions is required [2–5,8,9].

In addition to system parameters such as flow rate, pressure, diameter, and inlet subcooling, much effort [21–34] has been devoted in recent years to surface influences on boiling heat transfer and critical heat flux. Frost and Kippenhan [21] first showed the influence of surface tension on boiling heat transfer by adding surface active agents to the bulk fluid in order to reduce surface tension at the heater surface, yielding an enhancement of the heat transfer. Kandlikar [22] developed a pool boiling model that incorporated the influence of surface wettability using data on vertical pool boiling with multiple wettability surfaces and working fluids. The developed model is an adaptation of Zuber's [15] model with coefficients involving contact angle. However, the predicted value for CHF decreases to zero as the contact angle approaches 180°. Hsu and Chen [23] studied the effect wettability had on boiling heat transfer with nano-silica particle coatings on a copper surface in a horizontal pool boiling system. The CHF was observed to decrease with increasing contact angle, and pool boiling curves shifted to greater wall superheat with increasing contact angle, thus degrading the heat transfer in the nucleate boiling regime. Large differences were also observed in the wall nucleation phenomenon between the different wettability surfaces. Li et al. [24] performed a theoretical analysis and an experimental study on the influence of wettability on boiling properties in pool conditions for hydrophilic surfaces. A semi-analytical model employing correlations involving wettability for the departure frequency, diameter, and site density were used to calculate the latent heating of the heater surface, and the model was shown to predict the heat flux within 30% for several hydrophilic surfaces with varying wettabilities in pool boiling. Bourdon et al. [25] also studied the influence of wettability on boiling heat transfer and onset of nucleate boiling, performing horizontal pool boiling studies on smooth glass surfaces. The wettability was controlled with chemical grafting, thereby not modifying the surface topography, obtaining two surfaces: hydrophilic and hydrophobic. The less wetted (hydrophobic) surface was found to have an earlier ONB point compared with the other surface, and the pool boiling curve was found to be shifted to lower wall superheat, though CHF was not investigated. Betz et al. [26] studied the heat transfer and wall nucleation from superhydrophobic, superhydrophilic, biphilic, and superbiphilic surfaces under pool boiling. The surfaces were prepared using silicon wafers and oxygen plasma to make the surfaces superhydrophilic. A thin layer of Teflon fluoropolymer was then spun onto select surfaces to create a superhydrophobic finish. It was observed that the nucleation site density increased with decreasing wettability (increasing contact angle) for the same wall superheat, which indicated an enhancement of the heat transfer coefficient for hydrophobic and superhydrophobic surfaces, a finding confirmed by the reported pool boiling curves. Jo et al. [27] also observed a similar effect on the pool boiling curves with a higher heat transfer coefficient for hydrophobic surfaces at low wall superheat and a higher heat transfer coefficient for hydrophilic surfaces at high wall superheat. The surfaces were prepared in a similar manner to those by Betz et al. [26] using a silicon dioxide surface for the hydrophilic surface and a Teflon surface for the hydrophobic surface. Both Betz et al. [26] and Jo et al. [27] observed lower CHF values for hydrophobic surfaces compared with hydrophilic surfaces and an enhancement of the CHF for biphilic or mixed-wettability surfaces. Marcel et al. [28] modeled the effect wettability has on the boiling characteristics through contact angle and the departure diameter using a stochastic-automata model in pool boiling. The nucleation site density is greater at the same wall superheat for less wetting surfaces which causes the heat flux to be greater. Kim et al. [29] studied the effect of surfaces with temperature varying wettabilities on the boiling heat transfer in vertical flow. Surfaces became more hydrophilic at higher temperatures, and boiling curves were shifted to lower wall superheat as the wettability increased. Kumar et al. [30] observed the opposite trend, decreasing wettability shifts boiling curves to lower wall superheat using copper surfaces coated with diamond or carbon nanotubes, thus changing the wettability. The CHF increased with increasing flow rate, but also increased with the carbon nanotube surface, which has a lower wettability than the plain copper surface, an effect also not observed by previous studies.

From a review of literature, although some effort has been made in pool conditions, few studies have systematically analyzed the effect of wettability on heat transfer and CHF in flow boiling. The objectives of this paper are to meet the data needs for improved understanding of the influence of surface characteristics on heat transfer and CHF in flow boiling and to evaluate the prediction capability of existing CHF models.

2. Experimental approach

A closed-loop facility described in Ooi et al. [35] is modified slightly to measure boiling heat transfer and CHF and is shown in Fig. 1. A positive-displacement pump is used to drive distilled water through the test section at a constant rate. A bypass is connected in parallel with the rest of the section to decrease pressure oscillations and to keep the flow steady through the test section. Water driven by the pump passes through a 5 kW preheater which is used to heat the water to the appropriate inlet temperature to the test section. Water is then driven into the vertical test section, a schematic of which is shown in Fig. 1(b). The assembly is made of

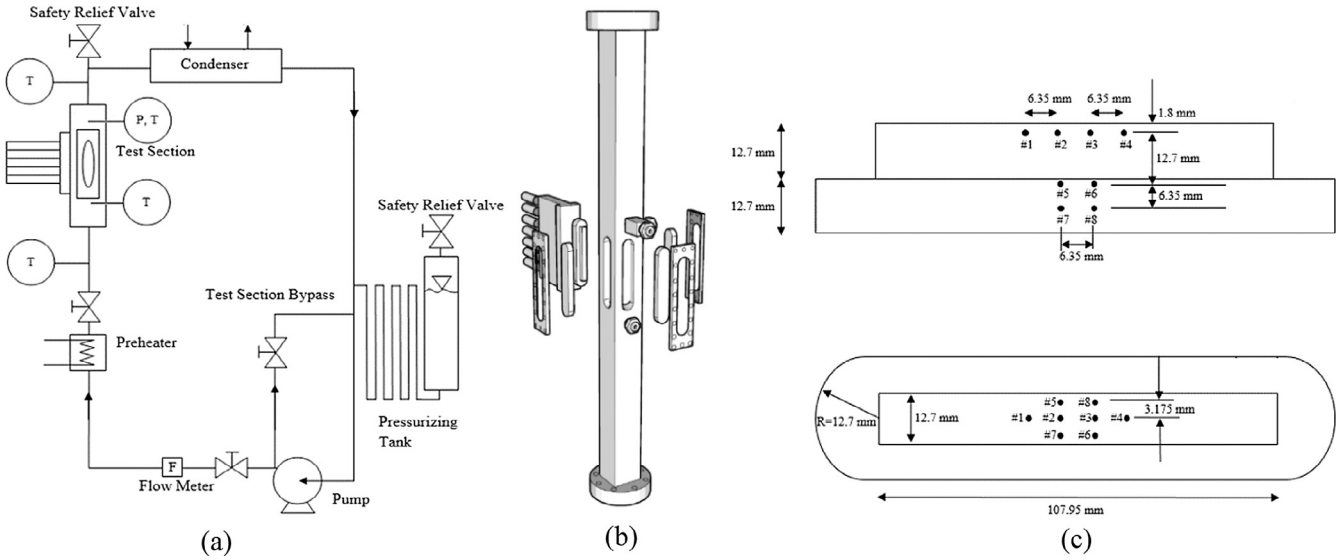

Fig. 1. Schematic of the facility showing (a) the facility layout, (b) the test section assembly, and (c) the heated surface and thermocouple configuration.

stainless steel except for the heater surface, Fig. 1(c), which is made of copper. The main section is a square channel of constant area throughout the entire assembly, measuring 12.7 mm × 12.7 mm. The unheated entry length is 490 mm followed by a one-sided heated section 107.95 mm long. The power is supplied by seven 750 W cartridge heaters connected to auto-transformers. Following the heated section, there is another 400 mm unheated section before the flow enters the condenser. The condenser cools the water to facilitate steady-state operation of the test facility. The condenser is a brazed plate heat exchanger which uses tap water on the secondary side to cool the distilled water moving through the test facility. The water then returns to the inlet of the pump, creating a closed loop.

A pressurizing tank is connected between the outlet of the condenser and the inlet of the pump. Winding vertical tubes separate the pressurizing tank from the apparatus to prevent non-condensable gases from entering the test section from the tank. The pressurizing tank is filled partially with distilled water, leaving the upper portion of the tank filled with compressible gas. A nitrogen tank and regulator are connected to the upper portion of the tank to control the system pressure. The pressurizing tank is used to control the system pressure, and it also acts to dampen pressure fluctuations.

The flow rate is measured using a turbine flow meter downstream from the pump. The flow rate is adjusted by using the controller for the pump motor and by opening and closing the main flow control valve upstream of the main test section. The bulk fluid temperature to the test section is controlled with a PID controller connected to the preheater based on a K-type thermocouple downstream from the preheater but upstream from the inlet to the test section assembly. Four T-type thermocouples are used within the stainless-steel test section to monitor the bulk fluid temperature at various locations. The thermocouples are placed at the beginning and end of each unheated section. The pressure transducer is connected at the end of the heated section to monitor the system pressure.

To monitor the heat flux and wall temperature of the heater surface, thermocouples are embedded into the heater surface at various depths, as shown in Fig. 1(c). Using a linear regression, the heat flux is determined by calculating the temperature gradient, using the thermal conductivity of copper, and assuming one-dimensional heat conduction. Additionally, the wall temperature is extrapolated from the temperature profile. The heat flux and wall temperature are then used to create the boiling curves for each condition.

Conditions were set for three target pressures: 100 kPa, 225 kPa, and 350 kPa. At each of these pressures, several flow rates were set ranging from approximately 50–300 kg/m^2-s. At each flow rate, experiments were performed where the inlet was very close to saturated liquid. The two T-type thermocouples upstream from the heated section were used to ensure that the liquid entering the heated section was close to saturation but not in the two-phase region. In addition, at pressures of 100 kPa and 225 kPa, CHF excursions at several subcoolings were studied. At 100 kPa, the inlet subcooling ranged from nearly saturation to 10 °C, while at 225 kPa the inlet subcooling ranged from nearly saturation to 15 °C. Table 1 shows the range of experimental measurements and associated uncertainty in the conditions studied.

Flow boiling experiments up to CHF were performed for two surfaces: a polished copper surface and a copper surface textured to make the surface wettability hydrophobic. The copper was polished with 1500-grit SiC paper and washed with water and acetone. A Coherent Monaco femtosecond diode-pumped laser system with linearly polarized light was used for the laser surface texturing of the copper heater with a method similar to that given by Hammouti et al. [36]. This laser operates at a central wavelength of 1040 nm (Full Width at Half Maximum), a pulse length of 350 fs, and a maximum power of 40 W when repetition rate is set at 1 MHz. A dual-axis galvo system and an F-Theta lens with an effective focal length of 160 mm were used to steer and focus the beam over the surface. The maximum field size is 110 mm × 110 mm with an uncertainty of 15 μrad. A schematic representation of the setup developed to perform 2D laser surface texturing is shown in Fig. 2(a).

Table 1
Range of measured conditions and associated uncertainty.

Experimental parameters	Values	Experimental uncertainty[a]
Pressure	106.0–360.2 kPa	±0.28 kPa
Inlet subcooling	0.2–15.7 °C	±0.1 °C
Wall superheat	0.5–23.8 °C	±0.22 °C
Mass flux	44–300 kg/m^2-s	±0.05 kg/m^2-s
Heat flux	25–1291 kW/m^2	±6.6 kW/m^2

[a] Based on steady-state time-averaged points.

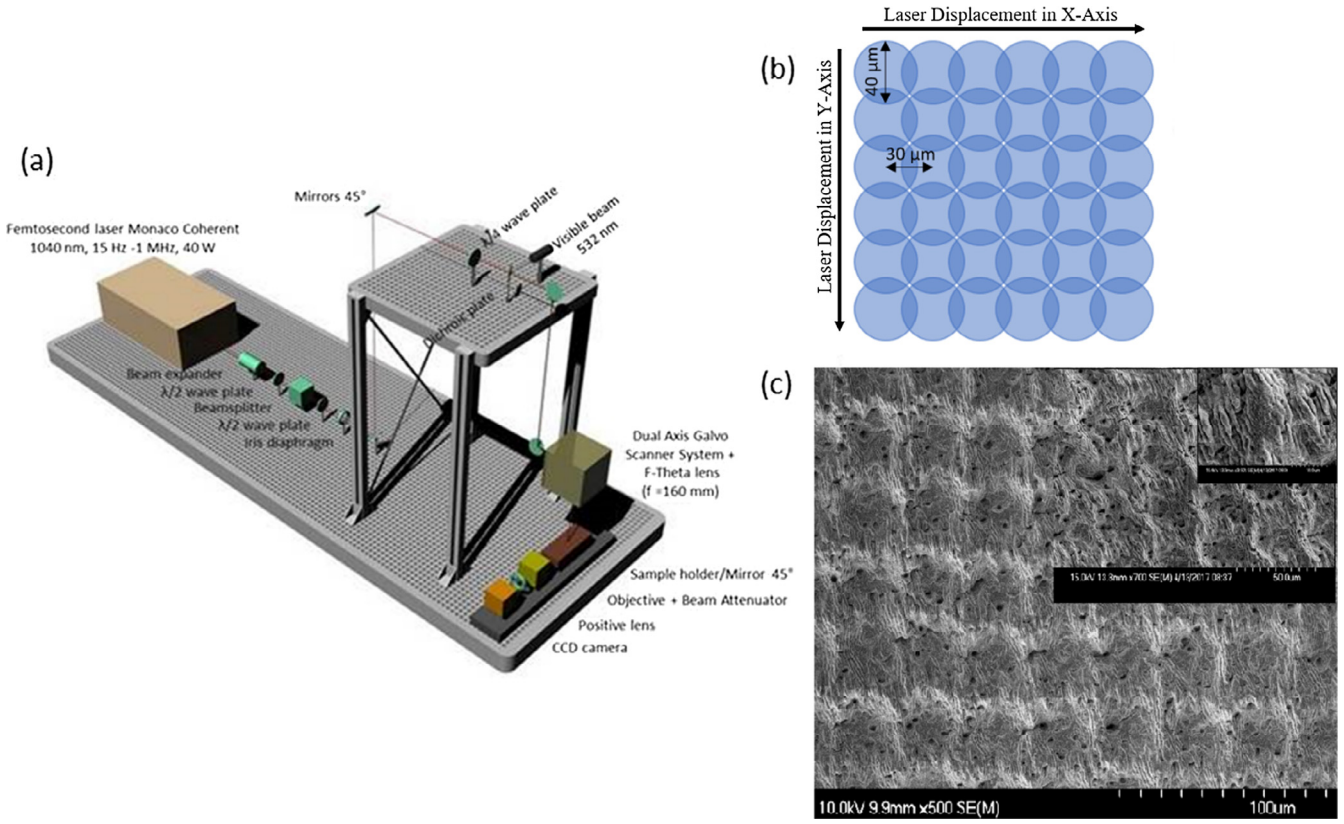

Fig. 2. (a) Schematic representation of the setup used to perform 2D laser surface texturing. (b) The surface texturing process of the copper heater surface. (c) 20° tilted SEM image of the surface after laser treatment, inset: magnified view of the rippled topography present inside the trenches.

Software was developed in LabVIEW in order to control the pattern of the texturing based on an imported image. The scale of the image is directly related to the distance between impacts in both the x and y axes, and the number of pulses per spot corresponded to the value of each pixel which compose the image. The laser spot size was found to be approximately 40 µm. Laser power was measured and set to 10 W before the laser surface texturing by means of a high-damage-threshold power detector just after the F-theta lens which leads to a fluence of 3.2 J/cm^2.

The copper surface was textured by a one-step laser process by keeping constant the lateral displacement of the laser spot at 30 µm in both the x and y directions. At each spot, 7000 fs pulses were delivered with a 1 MHz repetition rate. As shown in Fig. 2(c), the surface which was irradiated by laser presents self-organized periodic nanostructures called ripples or LIPSS (Laser-Induced Periodic Surface Structures) [37]. The combination of these nanostructures and the pad-like microstructures act as a multi-scale topography and is ideal for applications where hydrophobicity is required.

Wettability images were taken before each surface was subjected to the twenty-one conditions as well as after to ensure the wettability did not change throughout the experiment. The surface wettability was characterized with Sessile drop experiments, which were repeated twenty times for each surface. The average was computed for each surface: for the polished copper surface, the measured contact angle was found to be 58.7°, and the measured contact angle for the textured surface was found to be 131.9°. Examples of pictures from the drop experiments are shown in Fig. 3. A three-dimensional optical profiler was used to characterize the surface roughness of the polished and textured surfaces. As a result of the texturization, the surface roughness (arithmetic mean roughness) changed from an average value of 0.20 µm to 0.85 µm, and the roughness factor (defined as the ratio of the actual solid area to the projected area) changed from 1.077 to 1.454.

3. Results and analysis

A total of twenty-one test conditions were performed for each copper surface with variations in the system pressure, flow rate, and inlet subcooling. The heat flux was increased in small increments until CHF was detected by a sudden increase in the wall temperature and a sudden decrease in downstream liquid temperature. An example of the power profile for a condition is shown in Fig. 4. The reported critical heat flux values are determined by calculating the time derivative of the wall superheat for the entire condition. A running average is then applied to the derivative to more clearly identify the point of critical heat flux from the large volume of data collected for a particular condition. The CHF is taken as the point where the derivative deviates from zero immediately before the peak in the time derivative of the wall temperature. All data after the CHF excursion is ignored due to the rapid transient nature of the phenomenon and the fact that system properties are changed in order to cool the system quickly. The data for CHF are presented along with the conditions in Table 2.

3.1. Flow boiling curves

The boiling curves in Figs. 5–7 show three different types of data: steady-state points, running-average boiling curves between the steady-state points, and CHF excursion points. The steady-state points are depicted with markers. At these points, the heat flux and wall superheat are held constant after the system has had enough time to equilibrate to the wall heat flux, and the points shown are

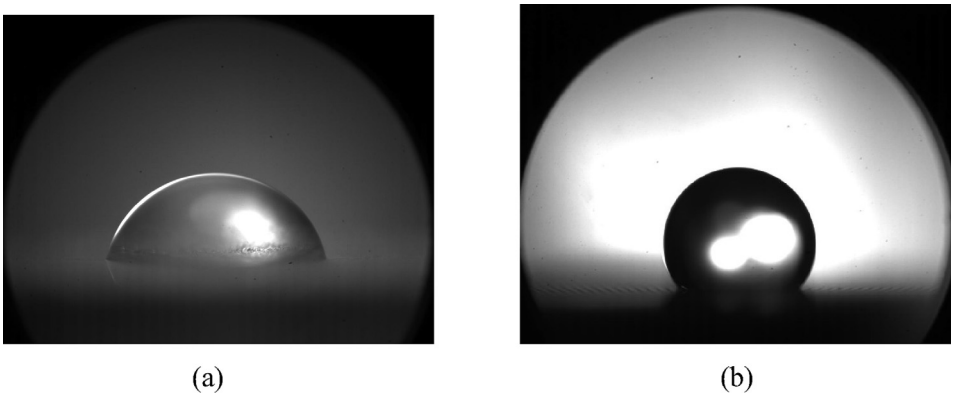

Fig. 3. Contact angle measurements on the two copper surfaces: (a) polished (hydrophilic), and (b) textured (hydrophobic).

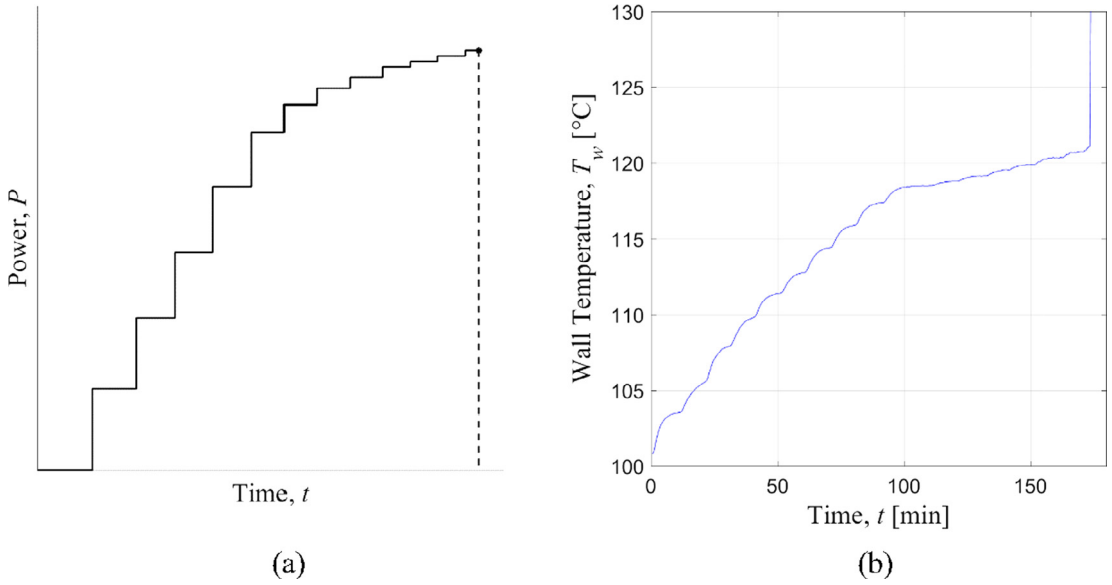

Fig. 4. Sample input and output for a run to CHF: (a) input of stepwise power input to cartridge heaters and (b) variation in wall temperature up to the temperature excursion point marking DNB.

Table 2
Data table with nominal reference, parameters, and critical heat flux values.

Nominal reference	P (kPa)	G (kg/m^2-s)	ΔT_{sub} (°C)	q''_{CHF} (kW/m^2)	Nominal reference	P (kPa)	G (kg/m^2-s)	ΔT_{sub} (°C)	q''_{CHF} (kW/m^2)
Hydrophilic surface					*Hydrophobic surface*				
1-i	106.1	49.9	1.4	496	1-o	107.6	49.6	1.8	470
2-i	106.0	50.3	5.0	661	2-o	107.5	49.5	5.3	464
3-i	106.4	46.6	10.0	717	3-o	107.8	48.1	10.1	431
4-i	106.6	95.4	1.4	594	4-o	108.6	96.0	1.8	504
5-i	106.8	95.0	5.0	720	5-o	108.6	94.8	5.0	509
6-i	106.9	94.0	10.0	788	6-o	108.2	94.4	10.1	493
7-i	109.1	187.5	1.5	681	7-o	109.9	187.9	1.9	523
8-i	108.5	188.1	5.1	818	8-o	109.6	188.8	5.2	556
9-i	108.2	187.6	10.0	915	9-o	108.9	188.5	10.0	607
10-i	225.5	94.1	4.9	886	10-o	227.1	93.2	5.3	614
11-i	226.5	92.1	15.2	998	11-o	226.3	93.7	15.1	611
12-i	229.0	184.5	5.4	992	12-o	226.4	185.5	5.2	636
13-i	225.8	185.0	15.0	1070	13-o	225.3	188.1	15.0	697
14-i	228.8	239.7	5.3	1014	14-o	225.4	241.5	5.0	704
15-i	229.6	239.5	15.4	1290	15-o	224.9	244.0	14.9	734
16-i	227.7	293.9	5.2	1070	16-o	225.8	297.0	5.0	742
17-i	226.0	295.0	14.9	1291	17-o	225.5	299.5	15.0	682
18-i	358.0	91.5	1.1	829	18-o	360.2	92.8	1.4	717
19-i	354.1	182.5	0.4	908	19-o	355.5	183.4	1.2	688
20-i	352.7	235.5	0.7	982	20-o	353.3	237.6	1.4	728
21-i	357.4	290.3	1.0	1145	21-o	353.7	292.7	1.4	758

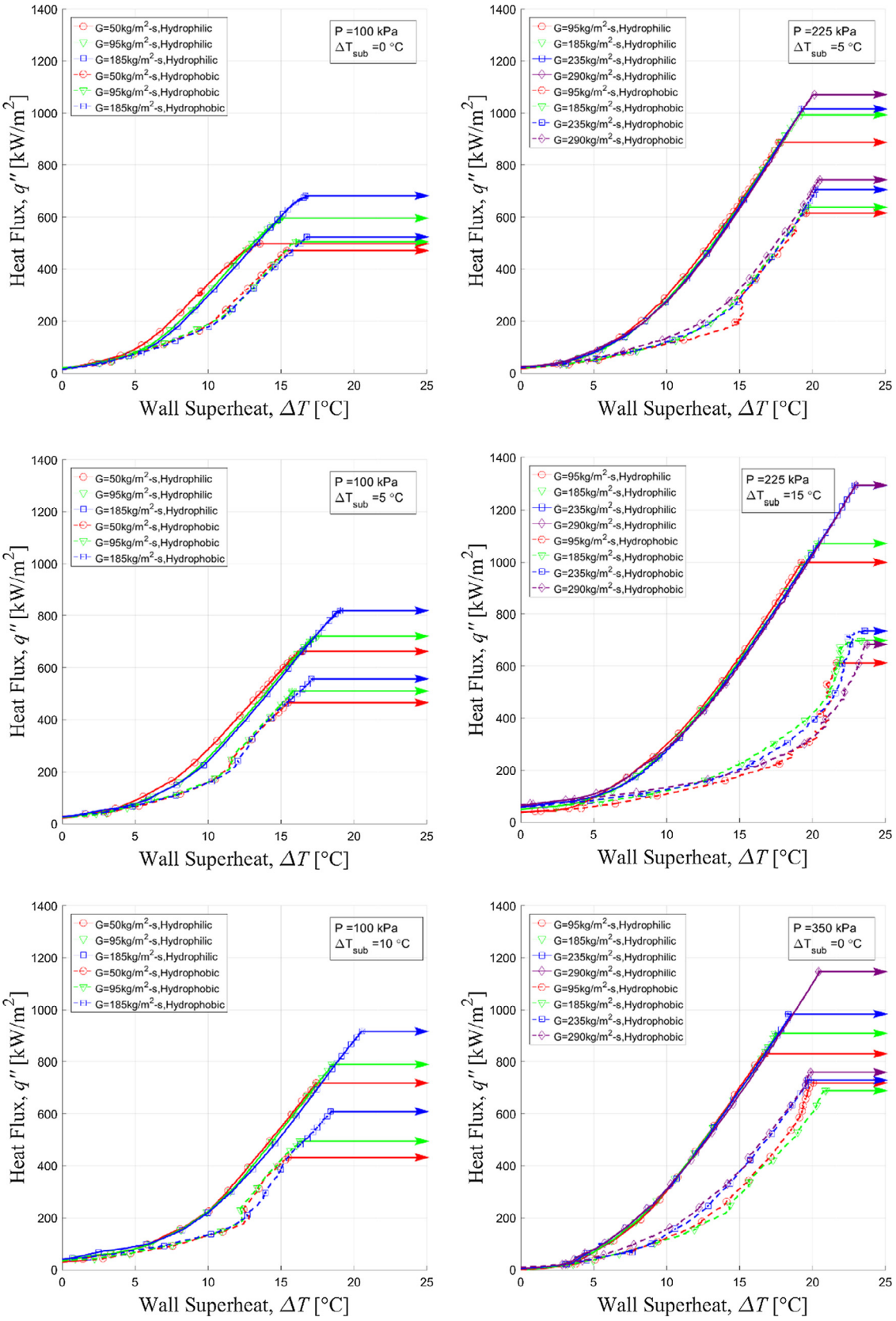

Fig. 5. Boiling curves and CHF excursions separated by flow rate for similar pressure and subcooling conditions for two wettability surfaces.

time-averaged quantities over two minutes. Next, the curves between the steady-state points are shown with solid or dotted lines. These are the boiling curves taken at 2 Hz with a running average over ten data points. Last, the CHF excursion points are shown with an arrow corresponding to the point where the temperature excursion begins.

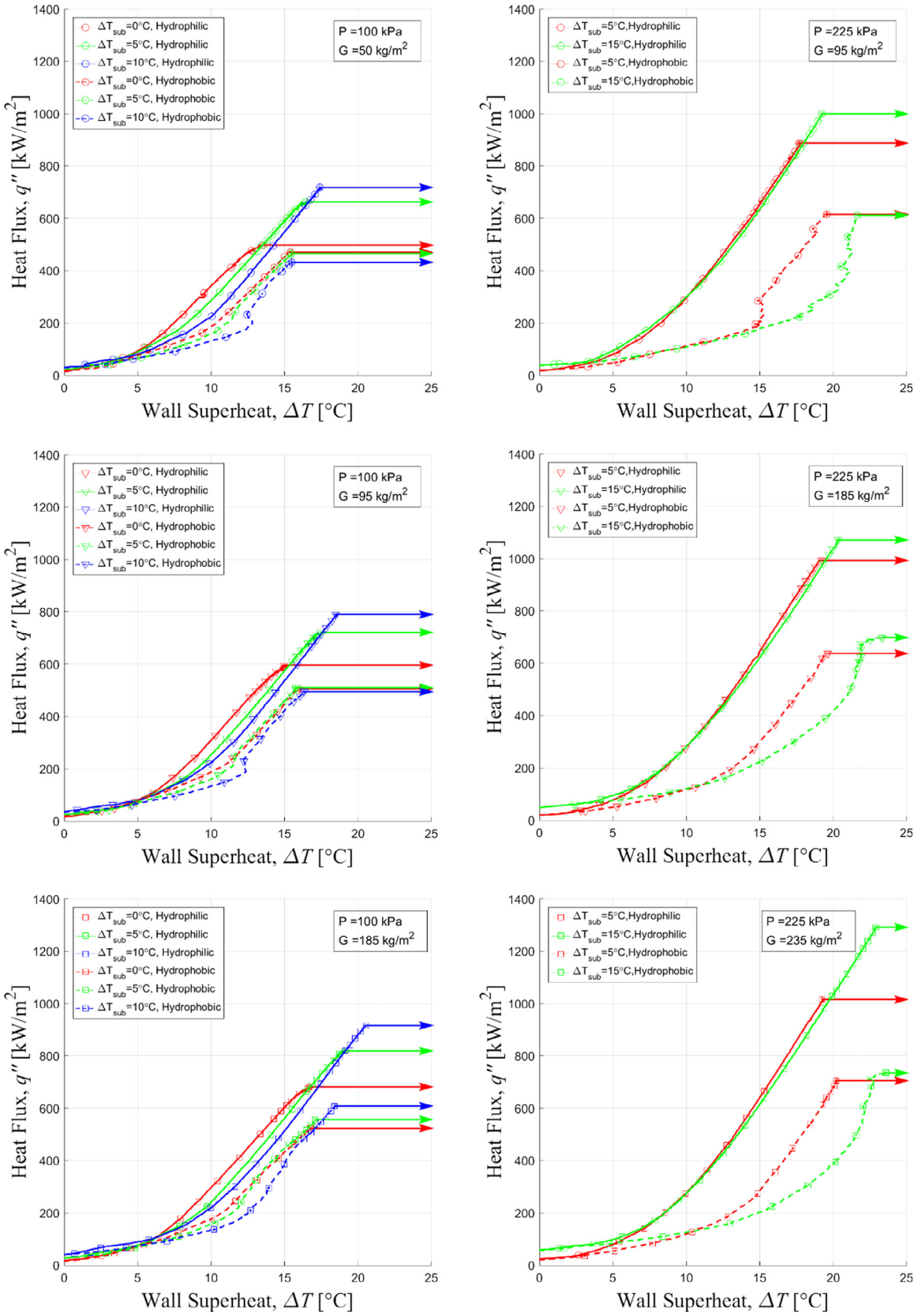

Fig. 6. Boiling curves and CHF excursions separated by subcooling for similar pressure and flow rate conditions for two wettability surfaces.

Fig. 5 shows various boiling curves separated by mass flux for both the hydrophilic (solid line) and hydrophobic surfaces (dashed line). The boiling curves for the hydrophilic surface are consistent across different flow rates for similar pressure and subcooling conditions. The only difference among the boiling curves for the hydrophilic surface is the location of the CHF point along the

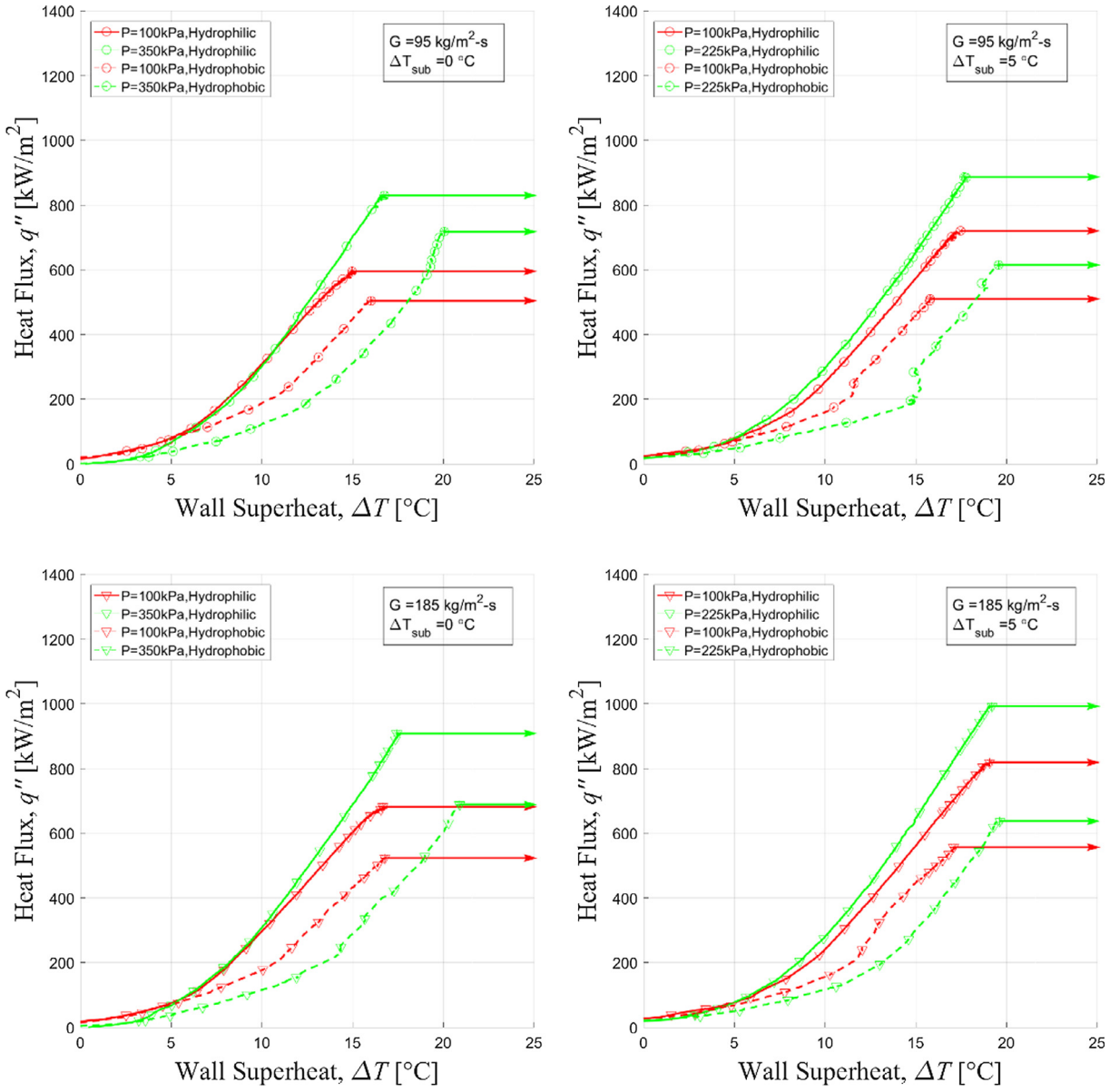

Fig. 7. Boiling curves and CHF excursions separated by pressure for similar flow rate and subcooling conditions for two wettability surfaces.

boiling curve in the nucleate boiling region. At elevated flow rates, the CHF is higher; however, the slopes of the boiling curves are nearly parallel, indicating similar boiling phenomenon. The hydrophobic surface boiling curves are shifted to the right as a result of a delay in the onset of nucleate boiling relative to the hydrophilic surface. The ONB point is determined qualitatively from a demonstrable change in the slope indicating a change from the single-phase convection region to the nucleate boiling heat transfer region. This effect of delaying the ONB point is most pronounced for the intermediate-pressure condition and does not change substantially across the range of subcooling considered. Decreasing surface wettability in pool boiling has been reported to shift the ONB point to lower wall superheat [25,26]; results in this study may be a consequence of the change in other surface properties or the effect of flow boiling. This difference in trend between pool and flow boiling should be investigated further. As with the hydrophilic surface, the effect of flow rate on the hydrophobic surface is shown as the temperature excursion is delayed and the CHF is greater at higher flow rates for the same pressure and subcooling conditions. However, for every condition tested, the CHF for the hydrophobic surface is lower than for the hydrophilic surface. This may be a consequence of the reduction in wettability, inhibiting the microlayer evaporation and the rewetting of the heater surface following bubble departure, leading to a lower heat flux before the CHF event is triggered, as theorized by Kandlikar [22].

The effect of subcooling on the boiling curves is different, however, and is shown in Fig. 6. For the hydrophilic surface at low pressure, increasing subcooling has the effect of delaying the ONB point, thus shifting boiling curves to the right. This result is most pronounced at low pressure. Elevated-pressure conditions also exhibit this trend, though the effect is not as prominent. The boiling curves continue parallel to one another indicating similar boiling phenomenon for different subcoolings with similar flow rate and pressure conditions for the hydrophilic surface. For the hydrophobic surface, a similar trend is observed with the delay of the ONB point and the shift of the boiling curves to the right with increasing subcooling. At lower pressure and lower flow rate,

the curves collapse on one another, and the subcooling has little effect beyond the ONB point. The CHF points are all similar for the hydrophobic surface at low mass flux, but at the higher mass flux of 200 kg/m^2-s the effect of subcooling is present on the CHF point. Likewise, for the hydrophobic surface at elevated pressures, greater subcooling delays the ONB point and shifts the curve to the right. At elevated-pressure conditions, the difference in the boiling curves between hydrophobic and hydrophilic surfaces is greater than at lower pressures. For the hydrophobic surface at elevated pressure, the effect of subcooling is not as influential on the CHF point as it is on the hydrophilic surface.

The boiling curves separated by pressure are shown in Fig. 7. For the hydrophilic surface, increasing pressure has the effect of shifting the boiling curve to the left and increasing the CHF point. However, for the hydrophobic surface, increasing pressure has the effect of shifting the boiling curve to the right and also increasing the CHF point. Pressure is the only of the three parameters studied to have the opposite effect on the boiling curves between the hydrophobic and hydrophilic surfaces. Flow rate and subcooling shift the CHF and the boiling curves in the same direction for the two wettabilities, but the boiling curves shift in different directions with increasing pressure depending on the wettability of the heater surface. The increase in CHF is substantial for both the hydrophilic and hydrophobic cases with increasing pressure.

3.2. Critical heat flux

Fig. 8 compiles the CHF values from the boiling curves to analyze the trend with individual system parameters. In each subfigure, different line colors and marker styles are used to separate the flow rates, pressures, and subcoolings for the cases tested. The CHF values are consistently lower for the hydrophobic surface compared to the hydrophilic surface, averaging a decrease of 28% for similar system and flow conditions. It has been widely observed in pool boiling experiments that decreasing wettability decreases the CHF [22,23,25–27,38], which was also observed in flow boiling

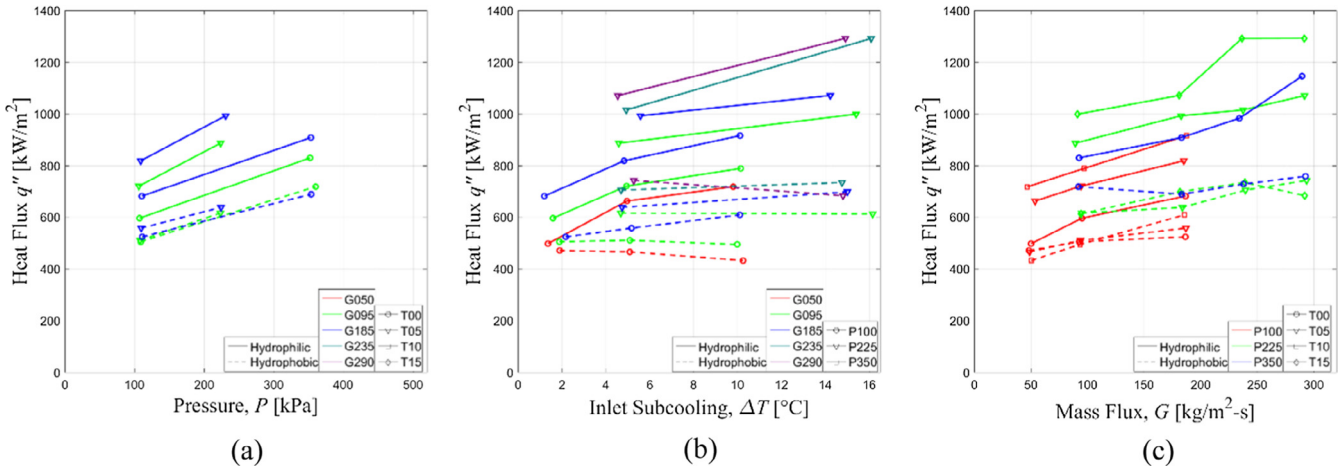

Fig. 8. Critical heat flux values versus system parameters, (a) pressure, (b) inlet subcooling, and (c) mass flux for the two wettability surfaces.

Table 3
Critical heat flux model comparison with experimental data.

Model	ε_{phil} (%)	ε_{phob} (%)	$\lvert\varepsilon_{phil}\rvert$ (%)	$\lvert\varepsilon_{phob}\rvert$ (%)
Kandlikar [22]	−1.0	64.2	19.5	64.2
Quan [32]	3.9	46.3	12.6	46.3
Thorgerson et al. [45]	−9.4	−50.4	23.5	50.5
Lu et al. [8]	26.8	0.2	26.8	21.5
RELAP5 [43]	−26.9	−72.8	28.5	72.8
TRACE [41]	−61.7	−118.8	62.8	118.8
Zuber [15]	−55.7	−110.0	55.7	110.0
Kutateladze [40]	−68.1	−126.8	68.1	126.8
Sudo et al. [46]	−71.8	−132.4	71.8	132.4
Mishima et al. [47]	−73.1	−134.5	73.1	134.5
Borishanskii [48]	−82.0	−146.0	82.0	146.0
Chang and Snyder [49]	−86.7	−152.3	86.7	152.3
Ivey and Morris [50]	−86.7	−152.3	86.7	152.3
Rohsenow and Griffith [51]	−96.0	−165.7	96.0	165.7
Zuber et al. [52]	−111.7	−193.8	111.7	193.8
Moissis and Berenson [53]	−114.2	−190.4	114.2	190.4
Wallis [20]	−141.9	−228.5	141.9	228.5
Mirshak et al. [54]	−162.4	−258.0	162.4	258.0
Katto [55]	−169.5	−280.9	169.5	280.9
Mishima and Ishii [56]	−185.6	−299.0	185.6	299.0
Janssen and Levy [57]	−314.8	−471.1	314.8	471.1
Jens and Lottes [58]	−364.5	−568.7	364.5	568.7
Biasi et al. [59]	−417.9	−577.7	428.7	596.2
Tong [60]	−638.5	−917.4	638.5	917.4
Bowring [61]	−679.4	−975.5	955.0	1360.8

experiments [33,34]. In contrast, the experiments of O'Hanley et al. [39] concluded that changes in roughness and wettability were minor and that significant CHF change was only through porosity. Of the system parameters, the critical heat flux is impacted the most by pressure for both surfaces but is also affected by subcooling and flow rate over the range of conditions studied. In Fig. 8(a), pressure is shown to be more influential on the CHF value for the hydrophobic surface than for the hydrophilic surface, and in some cases the CHF for the hydrophobic surface doubles from one to three-and-a-half atmospheres of system pressure. By comparison, the CHF for the hydrophilic surface is a strong yet more modest function of pressure. Although the CHF for the hydrophobic surface is a stronger function of pressure, the CHF for the hydrophilic surface is a strong function of both mass flux and inlet subcooling for the range of conditions studied, as shown in Fig. 8(b) and (c).

As a general trend within the range of conditions studied, CHF increasing with increasing pressure, subcooling, and mass flux has been long-accepted in flow boiling [2–9]. In addition, under low-flow conditions, inlet subcooling was found to not be a significant influence on CHF for annular geometries [3–5]. For the

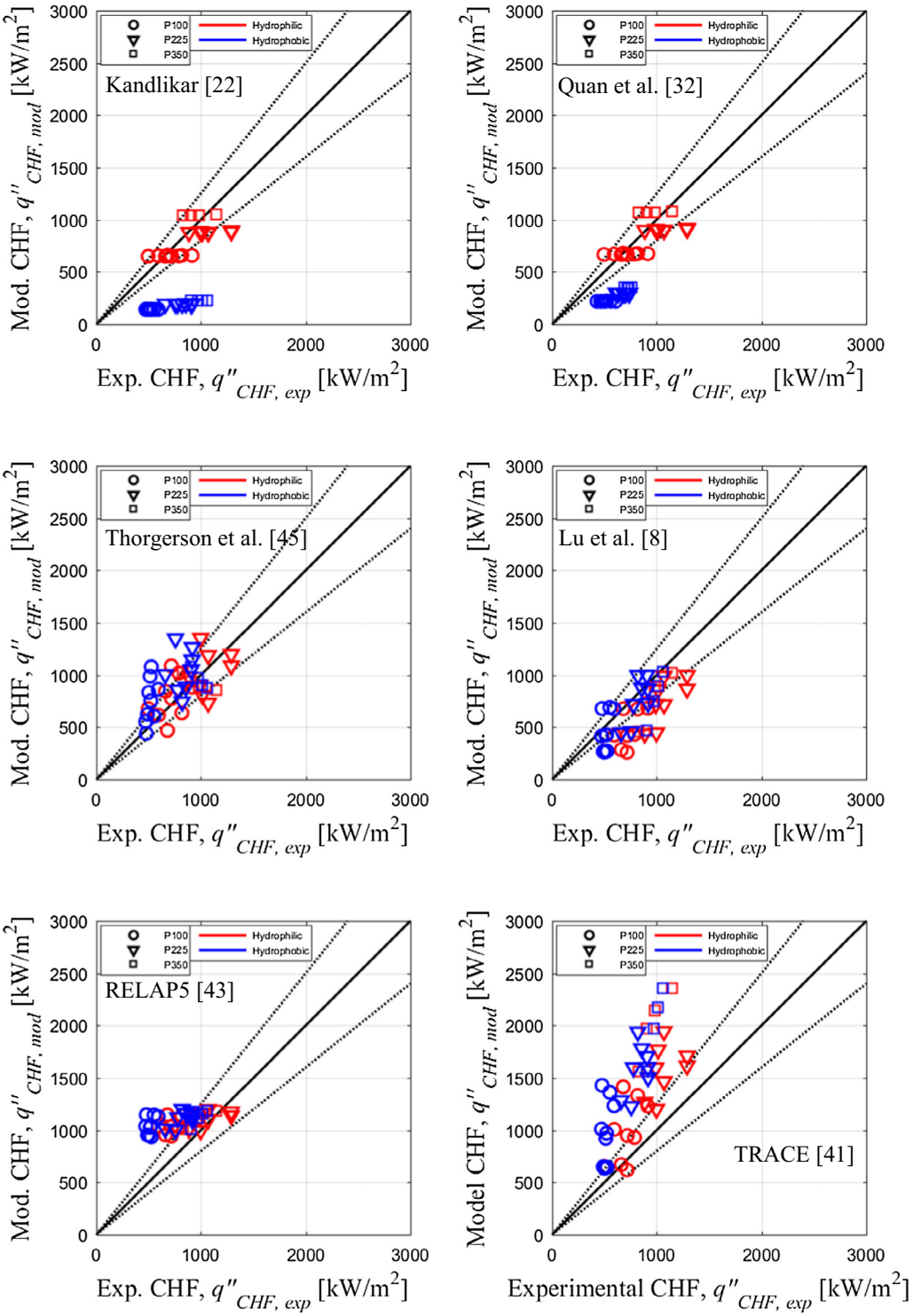

Fig. 9. Critical heat flux data comparison with top-performing models.

hydrophilic surface studied by Park et al. [6], a minor influence of subcooling on CHF was observed, but the dominant effect on CHF was found to be mass flux. In the present study, an independence of CHF with subcooling at low flow is only observed for the hydrophobic surface at the lowest pressure with a similar dependence on mass flux for both surfaces. This suggests the surface wettability influences the CHF transition not only in value but also in mechanism as the effect is not observed in the studied parameter range for the hydrophilic surface.

3.3. CHF model comparison

The critical heat flux data for both the hydrophilic surface and the hydrophobic surface are compared with available CHF models. The results are shown in Table 3 with mean errors and mean absolute errors for each data set. Many of the correlations are based on the semi-empirical models of Kutateladze [40] and Zuber [15] for pool boiling, so the effect of flow rate is not incorporated. Kandlikar [22] is the only model which incorporates contact angle, a model that is based on the pool boiling correlations of Kutateladze [40] and Zuber [15] as well. The correlation employed by TRACE [41] is a modified version of the Groeneveld [42] lookup table which, at low-flow conditions, interpolates CHF based on Zuber's [15] model. The model employed by RELAP5 [43] is based on correlations developed by the Nuclear Research Institute Rez in the Czech Republic [44]. The RELAP5 [43] model includes the effects of flow rate, pressure, quality, and inlet subcooling, but there is no influence of contact angle or surface effects.

Nearly all of the reported correlations overpredict the observed critical heat flux for both the hydrophilic and hydrophobic surfaces. Since contact angle is not considered in the models and since the observed critical heat flux is lower for the hydrophobic surface than the hydrophilic surface, the errors are larger for the hydrophobic surface. The only exceptions to this are the correlations by Kandlikar [22] and Lu [8]. The correlation by Kandlikar [22] includes contact angle, but the effect is exaggerated for poorly wetting surfaces, resulting in an underestimation of CHF for the hydrophobic surface. The data from which Kandlikar's [22] correlation is based varies contact angle only from 20° to 110° for pool boiling conditions, and the effect is extrapolated for superhydrophilic surfaces and more hydrophobic surfaces. The present study has a hydrophobic surface with a contact angle of 132°, which is outside the data range considered by Kandlikar [22]. The modification on Kandlikar [22] by Quan et al. [32] to include roughness is shown to improve the CHF prediction for the hydrophobic surface. Lu et al. [8] is the only reported correlation to underpredict the CHF for both the hydrophobic and hydrophilic surfaces. The correlation by Lu et al. [8] includes the effects of geometry, pressure, and flow rate, but does not include the influence of contact angle or inlet subcooling on the CHF value. The data off which the Lu et al. [8] correlation is based covers a similar parameter range to the current study; however, the geometry studied was an annulus with smaller hydraulic diameter and heated length. As discovered by El-Genk et al. [5], heater size has an influence on the CHF, albeit to a smaller degree, compared to the other system and flow parameters. Fig. 9 shows a comparison of the experimental data and the model data for the best six reported models. The data are separated by pressure as this is the most influential factor for many of the models. Both Thorgerson et al. [45] and RELAP5 [43] estimate the CHF values better than many of the other models. RELAP5 [43] incorporates the mass flux, exit quality, and pressure and overestimates the CHF value even for the hydrophilic surface and, therefore, overestimates the hydrophobic surface to a greater degree. The model by Thorgerson et al. [45] is an empirical model incorporating liquid velocity, pressure, and fluid temperature. Nearly every model implemented overestimates the critical heat flux, a real danger should these models be applied in low-pressure, low-flow systems. Even Kandlikar [22], which does incorporate contact angle, struggles to capture the effect of wettability for the studied hydrophobic surface. Additional flow boiling CHF models incorporating contact angle should be developed, but in that absence, the Lu et al. [8] model should be applied for conservative safety margins when operating within the range of conditions considered in this experimental study.

4. Conclusions

It is demonstrated that wettability plays a significant role in vertical boiling flow and influences various boiling characteristics. The ONB point is delayed for every condition studied for the hydrophobic surface compared with the hydrophilic surface. In addition, the CHF is lower for every condition for the hydrophobic compared with the hydrophilic surface, but similar trends are observed between conditions across surfaces such as similar boiling curves with changing mass flux and subcooling. Both surfaces exhibited a dependence between the CHF value and the mass flux and pressure; however, only the hydrophilic surface CHF value increased with increasing subcooling for the range of conditions considered.

Model comparisons demonstrate that CHF at these conditions can be predicted within about 20%. Models systematically overestimate the CHF point, and the only model that incorporate contact angle does not perform well. Given the catastrophic consequences that can accompany CHF, conservatism is necessary in applying these models. In summary,

- Wettability is an important property not typically accounted for in boiling models,
- The surface preparation, principally the contact angle, influence the ONB point and affect the CHF value substantially, and
- Conservatism is recommended when applying the CHF models to systems where the wettability may be changed.

Conflict of interest

The authors declared that there is no conflict of interest.

Acknowledgement

This material is based upon work supported under an Integrated University Program Graduate Fellowship, DOE Phase II SBIR/STTR (award number DE-SC0011851), and Starfire Industries LLC. The surface characterizations using the three-dimensional optical profiler were carried out in the Frederick Seitz Materials Research Laboratory Central Facilities, University of Illinois.

References

[1] M. Liu, N.R. Brown, K.A. Terrani, A.F. Ali, E.D. Blandford, D.M. Wachs, Potential impact of accident tolerant fuel cladding critical heat flux characteristics on the high temperature phase of reactivity initiated accidents, Ann. Nucl. Energy 110 (2017) 48–62.
[2] K. Mishima, H. Nishihara, Effect of channel geometry on critical heat flux for low pressure water, Int. J. Heat Mass Transf. 30 (6) (1987) 1169–1182.
[3] S.Y. Chun, H.J. Chung, S.K. Moon, S.K. Yang, M.K. Chung, T. Schoesse, M. Aritomi, Effect of pressure on critical heat flux in uniformly heated vertical annulus under low flow conditions, Nucl. Eng. Des. 203 (2001) 159–174.
[4] T. Schoesse, M. Aritomi, Y. Kataoka, S.R. Lee, Y. Yoshioka, M.K. Chung, Critical heat flux in a vertical annulus under low upward flow and near atmospheric pressure, J. Nucl. Sci. Technol. 34 (6) (1997) 559–570.
[5] M.S. El-Genk, S.J. Haynes, S.H. Kim, Experimental studies of critical heat flux for low flow of water in vertical annuli at near atmospheric pressure, Int. J. Heat Mass Transf. 31 (11) (1988) 2291–2304.

[6] C. Park, S.H. Chang, W.P. Baek, Critical heat flux for finned and unfinned geometries under low flow and low pressure conditions, Nucl. Eng. Des. 183 (1998) 235–247.
[7] H.C. Kim, W.P. Baek, S.H. Chang, Critical heat flux of water in vertical round tubes at low pressure and low flow conditions, Nucl. Eng. Des. 199 (2000) 49–73.
[8] D. Lu, Q. Wen, T. Liu, Q. Su, A critical heat flux experiment with water flow at low pressures in thin rectangular channels, Nucl. Eng. Des. 278 (2014) 669–678.
[9] G. Mayer, R. Nagy, I. Nagy, An experimental study on critical heat flux in vertical annulus under low flow and low pressure conditions, Nucl. Eng. Des. 310 (2016) 461–469.
[10] M. Lin, P. Chen, Photographic study of bubble behavior in subcooled flow boiling using R-134a at low pressure range, Ann. Nucl. Energy 49 (2012) 23–32.
[11] R.J. Weatherhead, Nucleate Boiling Characteristics and the Critical Heat Flux Occurrence in Subcooled Axial-Flow Water Systems, ANL-6675, Argonne National Laboratory, Argonne, IL, 1963.
[12] A.E. Bergles, W.M. Rohsenow, The determination of forced-convection surface-boiling heat transfer, J. Heat Transf. (1964) 365–372.
[13] J. Weisman, B.S. Pei, Prediction of critical heat flux in flow boiling at low qualities, Int. J. Heat Mass Transf. 26 (10) (1983) 1463–1477.
[14] D.D. Hall, I. Mudawar, Critical heat flux (CHF) for water flow in tubes–I. Compilation and assessment of world CHF data, Int. J. Heat Mass Transf. 43 (2000) 2573–2604.
[15] N. Zuber, Hydrodynamic Aspects of Boiling Heat Transfer, Ph.D. thesis, Research Laboratory, Los Angeles and Ramo-Wooldridge Corporation, University of California, Los Angeles, CA, 1959.
[16] C.H. Lee, I. Mudawar, A mechanistic critical heat flux model for subcooled flow boiling based on local bulk flow conditions, Int. J. Multiph. Flow 14 (6) (1988) 711–728.
[17] Y. Katto, A physical approach to critical heat flux of subcooled flow boiling in round tubes, Int. J. Heat Mass Transf. 33 (4) (1990) 611–620.
[18] J.E. Galloway, I. Mudawar, CHF mechanism in flow boiling from a short heated wall–II. Theoretical CHF model, Int. J. Heat Mass Transf. 36 (10) (1993) 2527–2540.
[19] I. Mudawar, A.H. Howard, C.O. Gersey, An analytical model for near-saturated pool boiling critical heat flux on vertical surfaces, Int. J. Heat Mass Transf. 40 (10) (1997) 2327–2339.
[20] G.B. Wallis, Flooding Velocities for Air and Water in Vertical Tubes, AEEW-R123, 1961.
[21] W. Frost, C.J. Kippenhan, Bubble growth and heat-transfer mechanisms in the forced convection boiling of water containing a surface active agent, Int. J. Heat Mass Transf. 10 (1967) 931–949.
[22] S.G. Kandlikar, A theoretical model to predict pool boiling CHF incorporating effects of contact angle and orientation, J. Heat Transf. 123 (2001) 1071–1079.
[23] C.C. Hsu, P.H. Chen, Surface wettability effects on critical heat flux of boiling heat transfer using nanoparticle coatings, Int. J. Heat Mass Transf. 55 (2012) 3713–3719.
[24] Y.Y. Li, Z.H. Liu, G.S. Wang, A predictive model of nucleate pool boiling on heated hydrophilic surfaces, Int. J. Heat Mass Transf. 65 (2013) 789–797.
[25] B. Bourdon, P.D. Marco, R. Rioboo, M. Marengo, J.D. Coninck, Enhancing the onset of pool boiling by wettability modification on nanometrically smooth surfaces, Int. Commun. Heat Mass Transf. 45 (2013) 11–15.
[26] A.R. Betz, J. Jenkins, C.J. Kim, D. Attinger, Boiling heat transfer on superhydrophilic, superhydrophobic, and superbiphilic surfaces, Int. J. Heat Mass Transf. 57 (2013) 733–741.
[27] H.J. Jo, H.S. Ahn, S.H. Kang, M.H. Kim, A study of nucleate boiling heat transfer on hydrophilic, hydrophobic and heterogeneous wetting surfaces, Int. J. Heat Mass Transf. 54 (2011) 5643–5652.
[28] C. Marcel, A. Clausse, C. Frankiewicz, A. Betz, D. Attinger, Numerical investivation into the effect of surface wettability in pool boiling heat transfer with a stochastic-automata model, Int. J. Heat Mass Transf. 111 (2017) 657–665.
[29] J.M. Kim, S.H. Kang, D.I. Yu, H.S. Park, K. Moriyama, M.H. Kim, Smart surface in flow boiling: spontaneous change of wettability, Int. J. Heat Mass Transf. 105 (2017) 147–156.
[30] C.S.S. Kumar, S. Suresh, L. Yang, Q. Yang, S. Aravind, Flow boiling heat transfer enhancement using carbon nanotube coatings, Appl. Therm. Eng. 65 (2014) 166–175.
[31] A.D. Sommers, K.L. Yerkes, Using micro-structural surface features to enhance the convective flow boiling heat transfer of R-134a on aluminum, Int. J. Heat Mass Transf. 64 (2013) 1053–1063.
[32] X. Quan, L. Dong, P. Cheng, A CHF model for saturated pool boiling on a heated surface with micro/nano-scale structures, Int. J. Heat Mass Transf. 76 (2014) 452–458.
[33] M.S. Sarwar, Y.H. Jeong, S.H. Chang, Subcooled flow boiling CHF enhancement with porous surface coatings, Int. J. Heat Mass Transf. 50 (2007) 3649–3657.
[34] S.J. Kim, L. Zou, B.G. Jones, An experimental study on sub-cooled flow boiling CHF on R134a at low pressure condition with atmospheric pressure (AP) plasma assisted surface modification, Int. J. Heat Mass Transf. 81 (2015) 362–372.
[35] Z.J. Ooi, V. Kumar, J.L. Bottini, C.S. Brooks, Experimental investigation of variability in bubble departure characteristics between nucleation sites in subcooled boiling flow, Int. J. Heat Mass Transf. 118 (2018) 327–339.
[36] S. Hammouti, B. Holybee, M. Christenson, M. Szott, K. Kalathiparambil, S. Stemmley, B. Jurczyk, D.N. Ruzic, Wetting of liquid lithium on fusion-relevant materials microtextured by femtosecond laser exposure, J. Nucl. Mater. 508 (2018) 237–248.
[37] R. Buividas, M. Mikutis, S. Juodkazis, Surface and bulk structuring of materials by ripples with long and short laser pulses: recent advances, Prog. Quant. Electron. 38 (2014) 119–156.
[38] S.P. Liaw, V.K. Dhir, Effect of surface wettability on transition boiling heat transfer from a vertical surface, in: Proceedings of the Eighth International Heat Transfer Conference, San Francisco, CA, vol. 4, 1986, pp. 2031–2036.
[39] H. O'Hanley, C. Coyle, J. Buongiorno, T. McKrell, L.W. Hu, M. Rubner, R. Cohen, Separate effects of surface roughness, wettability, and porosity on the boiling critical heat flux, Appl. Phys. Lett. 103 (2013) 024102.
[40] S.S. Kutateladze, Heat transfer in Condensation and Boiling, USAEC Report AEC-tr-3770, 1952.
[41] TRACE V5.840 Theory Manual: Field Equations, Solution Methods, and Physical Models, Division of Safety Analysis, Office of Nuclear Regulatory Research, U.S. Nuclear Regulatory Commission, Washington, DC, 2013.
[42] D.C. Groeneveld, L.K.H. Leung, P.L. Kirillov, V.P. Bobkov, I.P. Smogalev, V.N. Vinogradov, X.C. Huang, E. Royer, The 1995 look-up table for critical heat flux in tubes, Nucl. Eng. Des. 163 (1996) 1–23.
[43] RELAP3.3 MOD3.3 Code Manual Volume IV: Models and Correlations, Information Systems Laboratories, Inc., Rockville, Maryland, Idaho Falls, Idaho, 2010.
[44] R. Pernica, J. Cizek, General correlation for prediction of critical heat flux ratio, in: Proceedings of the 7th International Meeting on Nuclear Reactor Thermal-Hydraulics, NURETH-7, NUREG/CP-0142, vol. 4, Saratoga Springs, NY, 1995.
[45] E.J. Thorgerson, D.H. Knoebel, J.H. Gibbons, A model to predict convective subcooled critical heat flux, J. Heat Transf. 96 (1974) 79–82.
[46] Y. Sudo, K. Miyata, H. Ikawa, M. Kaminaga, M. Ohkawara, Experimental study of differences in DNB heat flux between upflow and downflow in vertical rectangular channel, J. Nucl. Sci. Technol. 22 (8) (1985) 604–618.
[47] K. Mishima, H. Nishihara, T. Shibata, CHF correlations related to the core cooling of a research reactor, in: Proc. Int. Mtg. on Reduced Enrichment for Research and Test Reactors, Tokai, Japan, 1983.
[48] V.M. Borishanskii, An equation generalizing experimental data on the cessation of bubble boiling in a large volume of liquid, Zh. Tekh. Fiz. 26 (1956) 452–456.
[49] Y.P. Chang, N.W. Snyder, Heat transfer in saturated boiling, Chem. Eng. Prog. 56 (30) (1960) 25–28.
[50] H.J. Ivey, D.J. Morris, On the Relevance of the Vapor-liquid Exchange Mechanism for Subcooled Boiling Heat Transfer at High Pressure, UKAEA, Winfrith, 1962.
[51] W.M. Rohsenow, P. Griffith, Correlation of Maximum Heat Flux Data for Boiling of Saturated Liquids, Massachusetts Institute of Technology, Division of Industrial Cooperation, 1955.
[52] N. Zuber, M. Tribus, J.W. Westwater, The hydrodynamic crisis in pool boiling of saturated and subcooled liquids, in: Proc. International Conference on Developments in Heat Transfer, ASME, New York, 1962.
[53] R. Moissis, P.J. Berenson, On the hydrodynamic transitions in nucleate boiling, J. Heat Trans. 85 (3) (1963) 221–229.
[54] S. Mirshak, W.S. Durant, R.H. Towell, Heat Flux at Burnout, Savannah River Laboratory, 1959.
[55] Y. Katto, General features of CHF of forced convection boiling in uniformly heated rectangular channels, Int. J. Heat Mass Transf. 24 (8) (1981) 1413–1419.
[56] K. Mishima, M. Ishii, Flow regime transition criteria for upward two-phase flow in vertical tubes, Int. J. Heat Mass Transf. 27 (5) (1984) 723–737.
[57] E. Janssen, S. Levy, Burnout Limit Curves for Boiling Water Reactors, General Electric Company, APED-3892, 1962.
[58] W.H. Jens, P.A. Lottes, Analysis of Heat Transfer, Burnout, Pressure Drop and Density Data for High-pressure Water, Argonne National Lab, ANL-4627, 1951.
[59] L. Biasi, G.C. Clerici, S. Garribba, R. Sala, A. Tozzi, Studies on burnout. Part 3, Energia Nucl. 14 (9) (1967) 530–536.
[60] L.S. Tong, Prediction of departure from nucleate boiling for an axially non-uniform heat flux distribution, J. Nucl. Eng. 21 (3) (1967) 241–248.
[61] R.W. Bowring, A Simple but Accurate Round Tube, Uniform Heat Flux Dryout Correlation over the Pressure Range 0.7 to 17 MPa, UKAEA, AEEW-R-789, 1972.